

RESEARCH

Open Access



Insight into antioxidant-like activity and computational exploration of identified bioactive compounds in *Talinum triangulare* (Jacq.) aqueous extract as potential cholinesterase inhibitors

Olakunle Bamikole Afolabi^{1*} , Oluwaseun Ruth Olasehinde² , Olutunmise Victoria Owolabi², Kikelomo Folake Jaiyesimi¹, Funmilayo Deborah Adewumi³, Olajumoke Tolulope Idowu³, Samson Olatunde Mabayoje⁴, Adejoke Olukayode Obajuluwa⁴ and Oghenerobor Benjamin Akpor⁴

Abstract

Background Recent reports have highlighted the significance of plant bioactive components in drug development targeting neurodegenerative disorders such as Alzheimer's disease (AD). Thus, the current study assessed antioxidant activity and enzyme inhibitory activity of the aqueous extract of *Talinum triangulare* leaf (AETt) as well as molecular docking/simulation of the identified phytonutrients against human cholinesterase activities.

Methods In vitro assays were carried out to assess the 2,2- azinobis (3-ethyl-benzothiazoline-6-sulfonic acid) (ABTS) cation radicals and cholinesterase inhibitory activities of AETt using standard protocols. High performance liquid chromatography coupled with diode-array detection (HPLC–DAD) was employed to identify compounds in AETt. Also, for computational analysis, identified bioactive compounds from AETt were docked using Schrodinger's GLIDE against human cholinesterase obtained from the protein data bank (<https://www.rcsb.org/>).

Results The results revealed that AETt exhibited a significant concentration-dependent inhibition against ABTS cation radicals ($IC_{50} = 308.26 \pm 4.36 \mu\text{g/ml}$) with butylated hydroxytoluene (BHT) as the reference. Similarly, AETt demonstrated a significant inhibition against acetylcholinesterase (AChE, $IC_{50} = 326.49 \pm 2.01 \mu\text{g/ml}$) and butyrylcholinesterase (BChE, $IC_{50} = 219.86 \pm 4.13 \mu\text{g/ml}$) activities with galanthamine as the control. Molecular docking and simulation analyses revealed rutin and quercetin as potential hits from AETt, having showed strong binding energies for both the AChE and BChE. In addition, these findings were substantiated by analyses, including radius of gyration, root mean square fluctuation, root mean square deviation, as well as mode similarity and principal component analyses.

Conclusion Overall, this study offers valuable insights into the interactions and dynamics of protein–ligand complexes, offering a basis for further drug development targeting these proteins in AD.

Keywords Cholinesterase inhibitors, *Talinum triangulare*, Phytonutrients, Alzheimer's disease, Drug development

*Correspondence:

Olakunle Bamikole Afolabi

afolabiob@abuad.edu.ng; afolabioblessed10@yahoo.com

Full list of author information is available at the end of the article



© The Author(s) 2024. **Open Access** This article is licensed under a Creative Commons Attribution 4.0 International License, which permits use, sharing, adaptation, distribution and reproduction in any medium or format, as long as you give appropriate credit to the original author(s) and the source, provide a link to the Creative Commons licence, and indicate if changes were made. The images or other third party material in this article are included in the article's Creative Commons licence, unless indicated otherwise in a credit line to the material. If material is not included in the article's Creative Commons licence and your intended use is not permitted by statutory regulation or exceeds the permitted use, you will need to obtain permission directly from the copyright holder. To view a copy of this licence, visit <http://creativecommons.org/licenses/by/4.0/>. The Creative Commons Public Domain Dedication waiver (<http://creativecommons.org/publicdomain/zero/1.0/>) applies to the data made available in this article, unless otherwise stated in a credit line to the data.

Introduction

Alzheimer's disease (AD) is a prevalent age-related neurodegenerative disease and a leading cause of dementia [1]. It is characterized by progressive memory loss and cognitive decline, due to a persistent neurodegeneration and brain atrophy [2, 3]. The prevalence of AD has been reported to range from 3% in individuals aged 65 years to 47% in those aged 85 years and older, affecting approximately 15 million people worldwide [4–6]. This disease has become a severe medical problem in modern society as the population increases [7]. Significantly, while fatalities from cardiovascular diseases and prostate cancer decreased between 2000 and 2015, there was a notable increase in deaths associated with AD [5, 8]. Studies have unveiled a decline in cholinergic neurons, resulting in both structural and functional impairment in AD [9, 10]. Likewise, there are signs indicating that the pathogenesis and advancement of AD are markedly affected by heightened oxidative stress and cholinergic dysfunction [11].

Acetylcholinesterases, AChE (EC 3.1.1.7) and butyrylcholinesterase, BChE (EC 3.1.1.8), are a group of serine hydrolases responsible for the hydrolysis of acetylcholine (ACh) and butyrylcholine (BCh) into choline and acetic acid or butyric acid [12, 13]. The hydrolytic actions of these cholinesterases (ChE) have been reported to alter the levels of the cholinergic system, resulting into imbalance or disturbance in cholinergic signaling systems essential for proper neurotransmission and cognitive functions [14]. Both enzymes exhibit approximately 65% structural homology, and BChE primarily assumes a supportive role and contributes to approximately 10% of the overall ChE activities, specifically within the temporal cortex [15]. Inhibition of the enzymatic activities of AChE and BChE are particularly significant in sustaining acetylcholine and its activity at cholinergic synapses for normal cognitive function in AD and other dementia disorders [13, 16].

Presently, investigations toward discovering new target drugs capable of preventing both the pathophysiology and progression of numerous human diseases are on going in the field of science [9]. The therapeutic approaches that involve inhibition of cholinesterase and proliferation of ROS/RNS have been reported as crucial measures in the management of AD [17]. Several AChE inhibitors including rivastigmine, galantamine, donepezil, memantine, among others are readily available and in use for clinical attention in AD condition [18]. These chemotherapeutic agents are symptomatic with a temporary relief from AD by elevating Ach level in the brain [19]. Recently, naturally-derived bioactive compounds from plants are widely being exploited for their varied range of biological interactions and activities [20, 21]. These compounds possess the ability to scavenge and

inhibit the production of reactive species via their tendency to donate electron and stabilize these electrophiles [22].

Talinum triangulare (*Tt*), waterleaf is a dicotyledonous plant belonging to the family *Talinaceae* and commonly grown in humid tropics with alternate, simple, and succulent leaves [23]. The plant is commonly utilized in the preparation of soups and other culinary delicacies [24]. Research studies have revealed that the plant is rich in natural compounds like flavonoids and polyphenols [25, 26]. The plant has exhibited a wide range of biological and pharmaceutical properties, including anti-inflammatory, anti-fungal, neuroprotective, and anti-bacterial activities [27–29]. Additionally, in our previous studies, we reported the antioxidant properties [30], and presence of a number of bioactive compounds identified from the aqueous extract of *Tt* [25]. However, there is a paucity of information on computational interactions of these compounds with AChE and BChE activities in the prevention/management of neurodegeneration diseases such as AD. Hence, this study aimed to explore the potential cholinesterase inhibitory activities of aqueous extract of *Tt* leave (AETt) as well as investigating computer-aided interactions of available bioactive components for possible drug-like hits using in vitro and insilico approaches.

Materials and methods

Chemicals and reagents used

The chemicals and reagents which include acetylcholine iodide, butyrylcholine iodide, galantamine (galantamine hydrobromide Reminyl[®]), 2,2'-azinobis (3-ethyl-benzothiazoline-6-sulfonic acid) (ABTS), butylated hydroxytoluene (BHT) Ellman's reagent (5,5'-dithiobis (2-nitrobenzoic acid), DTNB) were procured from Sigma-Aldrich, Inc., (Saint Louis, MO). Other reagents used in this experiment were of analytical grade and prepared using sterilized distilled water in all-glass apparatus.

Plant collection and processing

Fresh ariel leaves of *Tt* were purchased from the popular King's market in Ado-Ekiti, Ekiti State, Nigeria. A voucher sample was subsequently taken to the Department of Plant Science at Ekiti State University, Ado-Ekiti, Ekiti State, Nigeria, for authentication and identification. The sample was identified by a taxonomist in the department and assigned Herbarium number UHAE 2013/76, following thorough taxonomic investigations from the database.

Preparation of aqueous extract of *Talinum triangulare*

The leaves were properly washed and air-dried at room temperature (RT, 25 °C) for two weeks to obtain a

constant weight and pulverized to powdery form using automated blender. A quantity of 50 g of the powdered sample was extracted with 500 ml of distilled water for a period of 48 h and concentrated at 55 °C using water-bath to achieve AETt. Thereafter, different concentrations were prepared from a stock solution obtained from the resulting extract and then subjected to different bioassays.

Antioxidant activity of AETt using ABTS inhibitory assay

The ABTS cation radical scavenging ability assay of AETt was carried out according to the method described of Miller et al. [31] with minor modifications. A volume of 0.2 ml of the sample at various concentrations was mixed with 2.0 ml of a diluted ABTS radical cation solution (7 mM ABTS dissolved in 0.01 M PBS at pH 7.4). The reaction mixture was then allowed to stand at RT for 20 min, and the absorbance was immediately measured at 734 nm using a UV spectrophotometer. The ABTS free radical scavenging ability of AETt was calculated and expressed as percentage (%) inhibition with BHT as standard control using:

$$\text{ABTS cation scavenging ability (\%)} = (Abs_{\text{control}} - Abs_{\text{sample}}) / Abs_{\text{control}} \times 100$$

Where; Abs_{control} = Absorbance of the reaction mixture in absence of the extract (control).

Abs_{sample} = Absorbance of the reaction mixture (in presence of the extract).

Cholinesterase inhibitory activity assay

Cholinesterase (AChE and BChE) inhibitory activity assay of the AETt was performed using a colorimetric method as described by Ellman et al. [32]. The AChE/BChE activity was determined in a reaction mixture with total volume of 1 ml, comprising 0.1 M phosphate buffer (pH 8.0), 10 mM DTNB, 0.05 ml cytosol, and 150 mM acetylcholine iodide or butyrylcholine iodide in the presence/absence of the inhibitor (different concentrations of the extract and control). The reaction mixture was monitored for a change in absorbance at 412 nm using a UV spectrophotometer at RT for a duration of 3 min. Following the analysis, the inhibitory activity of the extract against AChE or BChE was calculated and expressed as a percentage inhibition of the control as follows:

$$\text{AChE/BChE inhibitory activity (\%)} = (Abs_{\text{control}} - Abs_{\text{sample}}) / Abs_{\text{control}} \times 100.$$

Where; Abs_{control} = Absorbance of the reaction mixture without the extract (control).

Abs_{sample} = Absorbance of the reaction mixture with the extract.

Determination of IC₅₀ values

The IC₅₀ value (µg/ml), representing the concentration of AETt required to cause 50% inhibition was determined through the utilization of a linear regression curve generated with Microsoft® excel 2016 as described by Afolabi et al. [9]. This curve was generated by plotting the percentage inhibition caused by the extract against different concentrations (µg/ml) of the extract used. The straight line equation ($y = mx + c$) derived from the curve plotted was used to determine the values, where y represented % inhibition at 50%; m, slope; x, concentration that caused 50% inhibition; and c, intercept.

In silico and molecular simulation studies

Preparation of protein targets and ligands

The X-ray crystal structures of human acetylcholinesterase (AChE) (PDB ID: 4EY7) and human butyrylcholinesterase (BChE) (PDB ID: 6QAE) were acquired from the Protein Data Bank (<https://www.rcsb.org/>). Subsequently,

the obtained structures were subjected to further preparation using the protein preparation wizard feature in Glide. Additionally, all compounds obtained from the HPLC–DAD analysis, as well as the standard drugs for individual targets (obtained from MedExpress and DrugBank), were prepared using LigPrep 2.4 software as reported by Mahmoud et al. [33]. The optimization process utilized the OPLS-2005 force field, which led to the generation of low-energy conformers for each ligand [34].

Molecular docking modelling using Maestro

The HPLC–DAD identified compound from the AETt, along with known inhibitors (drugs), were subjected to molecular docking into the AChE (PDB ID: 4EY7) and BChE (PDB ID: 6QAE) using Schrodinger's grid-based ligand docking with energetics (GLIDE) software version 5.8, following the method described by Halgren [35]. For docking ligands, the Glide 5.6 software's receptor grid generation module (GRGGM) was utilized to define the active sites. Grids were generated around the active sites of 4EY7 and 6QAE using receptors with a van der Waals

scale of 0.9 for non-polar atoms, and co-crystallized ligands were used as references. Two distinct docking

techniques were employed: standard precision (SP) and high precision (XP) to explore the binding modes of the compounds and known inhibitors for each target as described by Friesner [36].

Prime MM/GBSA calculation

The Prime/MM-GB/SA technique was employed to calculate the free energy of binding for a specific set of ligands to a receptor using the OPLS-AA force field and the generalized-Born/surface area (GB/SA) continuum solvent model as described below [37].

$$\Delta G_{\text{binding}} = \Delta E + \Delta G_{\text{solvation}} + \Delta G_{\text{SA}} \quad (1)$$

$$\Delta E = E_{\text{complex}} - E_{\text{protein}} - E_{\text{ligand}} \quad (2)$$

Where in (1 & 2) $\Delta G_{\text{binding}}$, binding free energy; ΔG_{SA} , free energy of surface area; $\Delta G_{\text{solvation}}$, solvation free energy (1); ΔE , free minimized energy; E_{complex} , E_{protein} , and E_{ligand} are the minimized energies of the protein–inhibitor complex, protein and inhibitor, respectively.

$$\Delta G_{\text{solvation}} = G_{\text{solvation}(\text{complex})} - G_{\text{solvation}(\text{protein})} - G_{\text{solvation}(\text{ligand})} \quad (3)$$

Where in (3); $G_{\text{solvation}(\text{complex})}$, $G_{\text{solvation}(\text{protein})}$, and $G_{\text{solvation}(\text{ligand})}$ are the solvation free energies of the complex, protein, and inhibitor (ligand), respectively:

$$\Delta G_{\text{SA}} = G_{\text{SA}(\text{complex})} - G_{\text{SA}(\text{protein})} - G_{\text{SA}(\text{ligand})} \quad (4)$$

Where in (4); $G_{\text{SA}(\text{complex})}$, $G_{\text{SA}(\text{protein})}$, and $G_{\text{SA}(\text{ligand})}$ are the complex, protein, and inhibitor surface area energies, respectively.

ADMET/ADME and druglikeness analysis

The SwissADME web tool and ADMETlab 2.0 were employed to predict the ADMET, druglikeness, and medicinal chemistry parameters of rutin and quercetin as described by Daina et al. [38]. The tool is accessible at <http://www.swissadme.ch/>.

Molecular dynamics simulation and RMSD analyses

The protein–ligand complexes of rutin and quercetin as obtained from the molecular docking step were subjected to molecular dynamics simulation (MDS) over 20 nano seconds (ns) using GROMACS software 2018 [39], in order to understand the effect of their binding on the structural stability and conformational flexibility of protein–ligand complexes.

Statistical analyses

Data were analyzed using GraphPad Prism 8.0 (Version 8, Software Program, GraphPad Prism Inc., San Diego, CA).

Results were presented as mean \pm SD. One-way analysis of variance (ANOVA) was used for the analyses, followed by Tukey's post-hoc test. Significant differences were considered at $p < 0.05$.

Results

Antioxidant property and cholinesterase inhibitory activities of the aqueous extract of *Talinum triangulare* (AETt) leave

Figure 1 shows the inhibitory activity of AETt against ABTS free cation radical. As shown in the result, AETt demonstrated a significant ($p < 0.05$) inhibition in a concentration-dependent manner against ABTS cation radical ($IC_{50} = 308.26 \pm 4.36 \mu\text{g/ml}$) compared to BHT ($IC_{50} = 48.23 \pm 0.18 \mu\text{g/ml}$) (Table 1).

Figure 2 a&b reveal inhibitory activities of the AETt against AChE and BChE activities. As shown in the results, AETt revealed a significant ($p < 0.05$) inhibition against AChE activity ($IC_{50} = 326.49 \pm 2.01 \mu\text{g/ml}$) compared to galanthamine ($IC_{50} = 57.36 \pm 0.04 \mu\text{g/ml}$) (Table 1), similarly, the extract had a higher inhibition against BChE activity ($IC_{50} = 219.86 \pm 4.13 \mu\text{g/ml}$) compared to galanthamine ($IC_{50} = 51.37 \pm 0.28 \mu\text{g/ml}$) in a concentration-dependent manner.

Molecular docking analyses

Figure 3 (a&b) represent the molecular mechanics/generalized born surface area value (MMGBSA) for (a) rutin dynamics binding to AChE; (b) quercetin dynamics binding to BChE. As indicated in Fig. 3a, MMGBSA analysis for rutin binding to AChE revealed energy components, including Van der Waals (VDWAALS) at $-49.77 \pm 2.45 \text{ kcal/mol}$, electrostatic (EEL) at $-28.47 \pm 2.27 \text{ kcal/mol}$, generalized born electrostatic (EGB) at $54.15 \pm 1.96 \text{ kcal/mol}$, and nonpolar solvation (ESURF) at $-6.60 \pm 0.35 \text{ kcal/mol}$. The calculated free energy of binding (ΔG_{gas}) was $-78.24 \pm 3.59 \text{ kcal/mol}$, with a significant solvation contribution (ΔG_{solv}) of $47.54 \pm 1.87 \text{ kcal/mol}$. The overall binding energy (ΔG_{total}) was $-30.70 \pm 3.05 \text{ kcal/mol}$. Similarly, for quercetin binding to BChE (Fig. 3b), the MMGBSA analysis yielded energy components, including VDWAALS at $-27.41 \pm 0.95 \text{ kcal/mol}$, EEL at $-20.07 \pm 2.55 \text{ kcal/mol}$, EGB at $33.86 \pm 1.88 \text{ kcal/mol}$, and ESURF at $-4.27 \pm 0.09 \text{ kcal/mol}$. The calculated ΔG_{gas} was $-47.48 \pm 2.93 \text{ kcal/mol}$, with a ΔG_{solv} of $29.59 \pm 1.81 \text{ kcal/mol}$. The overall ΔG_{total} was $-17.89 \pm 1.19 \text{ kcal/mol}$.

Figure 4 (A & B) show post-docking analyses of human AChE protein target in complex with rutin and scopolepin (reference drug). The 2D representation of the human AChE–rutin complex shown in the Fig. 4A (a) indicated SP (-14.34 kcal/mol), XpGscore (-14.37 kcal/mol) and MM-GBSA dG bind score of -73.21 kcal/mol . However,

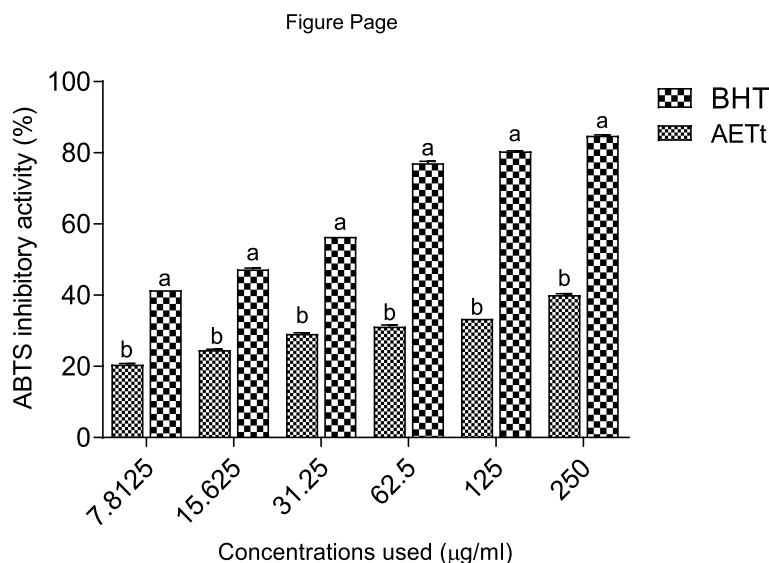


Fig. 1 ABTS inhibitory activity of the aqueous extract of *Talinum triangulare* leave. Key: **a** & **b** represent levels of significance at $p < 0.05$ among different concentrations used for the samples, i.e., across bars; *BHT* butylated hydroxytoluene, *AETt* aqueous extract of *Talinum triangulare* leave

Table 1 IC_{50} (µg/ml) of the inhibitory activities of AETt against ABTS, BchE and AchE

	AETt	Galanthamine	BHT
ABTS	308.26 ± 4.36	-	48.23 ± 0.18
AchE	326.49 ± 2.01	57.36 ± 0.04	-
BchE	219.86 ± 4.13	51.37 ± 0.28	-

Results represent mean ± SD of duplicate trials ($n = 2$)

in the Fig. 4B (a) scopoletin (reference drug) in complex with the same targets revealed SP (-7.91 kcal/mol), XpG-score (-7.92 kcal/mol) and MM-GBSA dG Bind score of -37.87 kcal/mol, respectively (Table 2). Also, as shown in Fig. 4A (b), the interaction of rutin (hit) with this target

showed twelve hydrogen bond formation at specific bond distances of TYR72 (1.7046), SER293 (2.43506), SER293 (1.75982), ARG296 (2.23347), ASP74 (2.80258), TRP286 (1.95637), GLN291 (2.24675), SER293(1.90847), TYR341 (1.96344), SER293 (2.72111), SER293 (2.19421), and PHE295 (3.22904), in addition to seven hydrophobic bond (Fig. 4A (c)) which included TYR341 (3.74547), TYR341 (3.80462), TYR124 (5.50253), TRP286 (4.86732), PHE338 (5.053), and PHE338 (5.53433), which are precisely alkyl, Pi-Pi T-shaped, and Pi-Pi Stacked. However, in contrast to the interactions formed by rutin with the same target, scopoletin interaction with the human AChE (Fig. 4B (b)) revealed the formation of three hydrogen bond interactions at specific bond distances

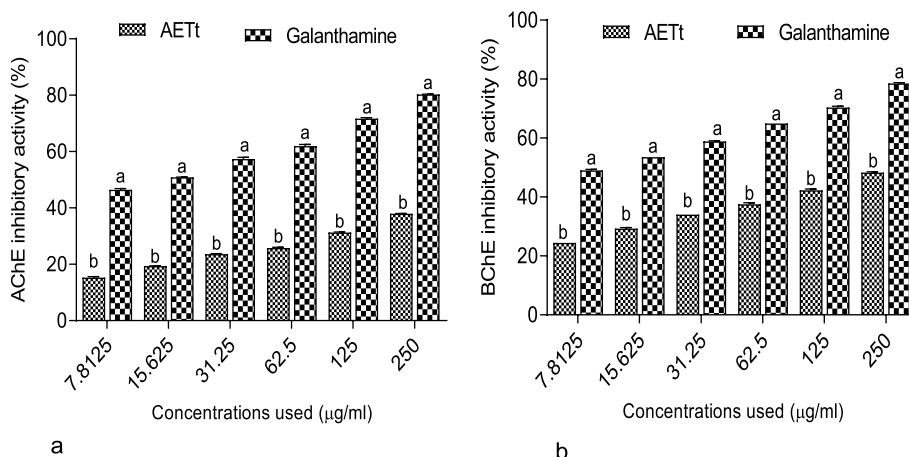


Fig. 2 Inhibitory activity of the aqueous extract of *Talinum triangulare* leave against **a** AChE and **b** BChE activities. Key: **a** & **b** represent levels of significance at $p < 0.05$ among different concentrations used for the samples, i.e., across bars; *AETt* aqueous extract of *Talinum triangulare* leave

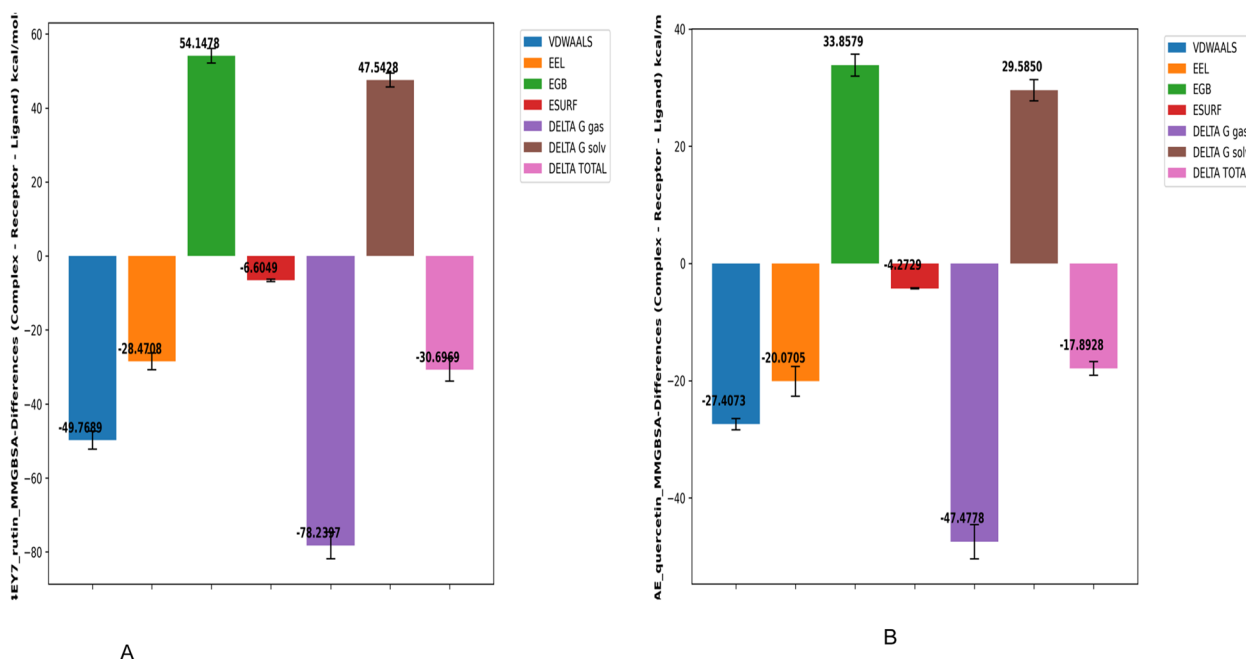


Fig. 3 a&b Molecular mechanics/generalized born surface area value (MMGBSA) for **a** rutin dynamics binding to AChE; **b** quercetin dynamics binding to BChE. Note: VDWAAL Van der Waals, EEL Electrostatic, EGB Generalized born electrostatic, ESURF Nonpolar solvation, DELTA G gas Calculated free energy of binding (ΔG gas), DELTA G Solv Solvation contribution, DELTA TOTAL overall binding energy (ΔG total)

of PHE295 (1.88968), VAL294 (2.70336), and TYR337 (2.95665), in addition to six hydrophobic bond interactions formed at TYR341 (3.93256), TYR341 (3.76354), PHE297 (5.88588), TRP86 (4.83487), TYR337 (5.07224), and TYR341 (5.4545), respectively (Fig. 4B (c)).

Figure 5 (A & B) show the post-docking analyses of human but BChE protein target in complex with quercetin and lycodoline (reference drug). The binding of human BChE protein target to quercetin as shown in Fig. 5A (a) revealed SP (-10.44 kcal/mol), XpGscore (-10.47 kcal/mol) and MM-GBSA dG bind score of -48.36 kcal/mol (Table 3). In contrast, lycodoline interaction with the same target as shown in Fig. 5B (a), indicated SP (-7.35 kcal/mol), XpGscore (-7.53 kcal/mol) and MM-GBSA dG bind score of -50.37 kcal/mol. Similarly, as shown in Fig. 5A (b) the interaction of quercetin with the human BChE revealed the formation of nine hydrogen bond interactions at specific bond distances of GLY116 (1.89663), GLY116 (2.46613), GLY117 (1.90848), SER198 (1.65067), LEU286 (1.9874), LEU286 (1.623), GLY115(2.63459), TRP82 (3.13666), and TRP82 (2.45968), in addition to the eight hydrophobic interactions formed at TRP82 (4.87994), TRP82 (5.34937), TRP231 (5.07094), TRP231 (4.88867), PHE329 (5.0448), HIS438 (4.51515), HIS438 (5.03233), LEU286 (5.09586) (Fig. 5A (c)). In contrast to the interactions formed with quercetin, interaction of lycodoline with human BChE (Fig. 5B (b)) revealed three hydrogen bond interactions

formed at specific bond distances of GLU197 (5.15888), TYR332 (2.85079), and SER79 (2.40171), in addition to five hydrophobic interactions formed at HIS438 (2.44777), TRP82 (4.94182), PHE329 (4.33196), TYR332 (4.91587), and TYR332 (3.59395), respectively (Fig. 5B (c)). These was in contrast to the interactions formed when Quercetin interact with the same target.

Molecular dynamics simulation analyses

Figure 6 represents radius of gyration (Rg) plot as a function of simulation time-dependent analysis of molecular dynamics trajectory of rutin and quercetin dynamics in complex with AChE and BChE. As indicated in the result, Rg values of the two apoproteins and their protein–ligand complexes in apo-AChE, AChE-rutin complex, apo-BChE and BChE-quercetin complex were 22.88320008, 22.78768594, 22.59427599 and 22.6976769, respectively.

Figure 7 (a&b) represent root mean square fluctuation of the residues of simulation time dynamics of (a) apo-AChE and AChE -rutin complexes; and (b) apo-BChE & BChE-quercetin complexes. As indicated in the plot, RMSF values of the two apoproteins and their protein–ligand complexes were apo-AChE (0.706342291), AChE -rutin (0.810035426), apo-BChE (0.705936449), and BChE-quercetin (0.733836349), respectively. Similarly, Fig. 8 represents the root mean square deviation (RMSD) plot as a function of simulation time of rutin and quercetin dynamics

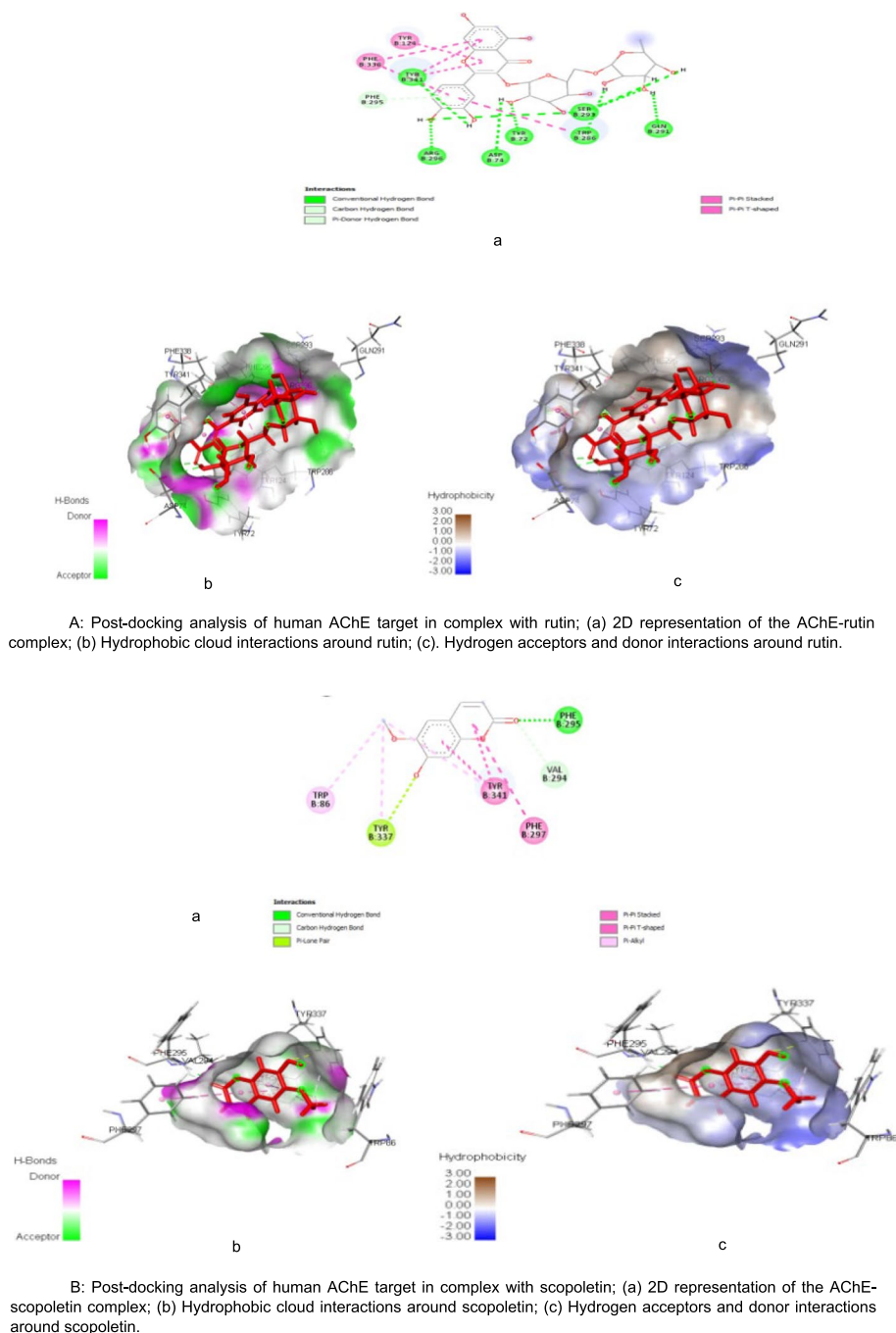


Fig. 4 **A** Post-docking analysis of human AChE target in complex with rutin; a 2D representation of the AChE-rutin complex; b Hydrophobic cloud interactions around rutin; c. Hydrogen acceptors and donor interactions around rutin. **B** Post-docking analysis of human AChE target in complex with scopoletin; a 2D representation of the AChE-scopoletin complex; b Hydrophobic cloud interactions around scopoletin; c Hydrogen acceptors and donor interactions around scopoletin

binding to acetylcholinesterase and butyrylcholinesterase. As shown in the plot, the average RMSD values recorded for the apo-protein systems and protein–ligand complexes for apo-acetylcholinesterase, acetylcholinesterase-rutin, apo-butyrylcholinesterase, and butyrylcholinesterase-quercetin

complexes were 1.450951857, 1.284406342, 1.391370699, and 1.402250976, respectively.

Figures 9 and 10 represent a plot of the receptors’ PC1, PC2, PC3, and eigenvalues versus the corresponding eigenvector indices for the different modes of motion in

Table 2 Post docking SP, XPG and MMGBSA scores of compounds from the AETt against human acetylcholinesterase target with scopoletin as standard

PubMed IUPAC	Docking score	XPG score	MMGBSA dG binding score
Rutin	-14.34	-14.37	-73.21
Quercetin	-12.16	-12.19	-59.43
Luteolin	-11.71	-11.75	-57.76
Kaempferol	-10.69	-10.72	-45.85
Scopoletin	-7.91	-7.92	-37.87

AChE-rutin and BChE-quercetin complexes. As indicated in Fig. 9, for the AChE-rutin, PC1 had the highest variance with 22.13%, followed by PC2 with 6.3%, and PC3 with 4.78%. Similarly, for the BChE-quercetin (Fig. 10), PC1 had a lower variance of 14.02%, while PC2 and PC3 had higher variances of 9.35% and 5.45%, respectively.

Discussion

The utilization of medicinal plants has gained a significant attention due to their vital roles in the management of several human ailments [40]. In recent times, this has sparked immense interest in investigating the diverse bioactive compounds involved and mechanisms of their actions [41]. Hence, our study explored in vitro antioxidant and enzyme inhibitory properties as well as interactions of bioactive compounds from AETt with AChE and BChE activities.

It is noteworthy that oxidative stress, resulting from the proliferation of free radicals, has essentially been implicated in the pathophysiology of AD [42, 43]. However, a list of natural plants rich in bioactive constituents have been reported to exhibit antioxidative properties either by chelating, scavenging or inhibiting the initial of ROS [9, 44]. Previous studies have similarly established a compelling correlation between the ABTS decolorization assay and the antioxidant capability of medicinal plants [45, 46]. This decolorization is based on the ability of any compound to donate electrons and cause the inhibition of ABTS radical cations generated through chemical reduction [47]. Nonetheless, the current investigation reveals that AETt exhibited a remarkable reduction in ABT radicals (Fig. 1), suggesting the capability of the extract to donate electrons to water-soluble and chemically stable ABT, ultimately causing its reduction [48].

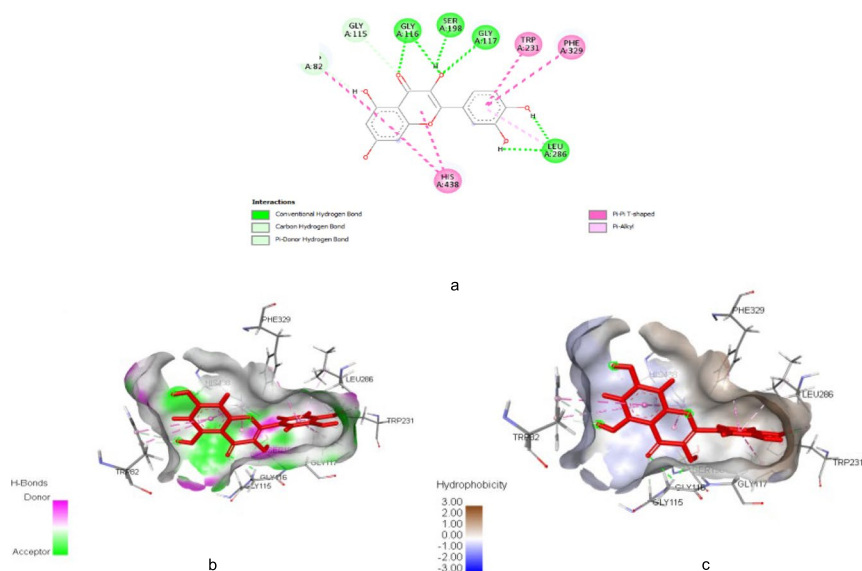
The cholinergic dysfunction, marked by exacerbated cholinesterase activities (AChE and BChE), is well recognized in Alzheimer's disease (AD), the most prevalent cause of dementia. [49]. Cholinesterase play a crucial role in the hydrolysis and depletion of ACh, a

neurotransmitter pivotal for cognitive and mental functions of the brain [2, 50]. Consequently, the inhibition of AChE and BChE has been documented as a significant strategy for managing AD, thus rendering it a pertinent target for the development of medications aimed at addressing AD [51]. Furthermore, recent studies have underscored the significance of medicinal plants in addressing AD as a result of the existence of bioactive secondary metabolites that have been identified as potential inhibitors of AChE and BChE [40, 52]. In our study (Fig. 2), it is evident that AETt exhibited a clear concentration-dependent inhibition of AChE and BChE activities, an effect that could probably be linked presence of compounds (Table S1 & Fig. S1) with the ability to donate H-atom (H^+), thus causing the inhibition of these hydrolyzing proteins at their catalytic sites [41]. As a result, it could be suggested that AETt holds the potential for neuroprotective effects valuable in the therapeutic management of AD.

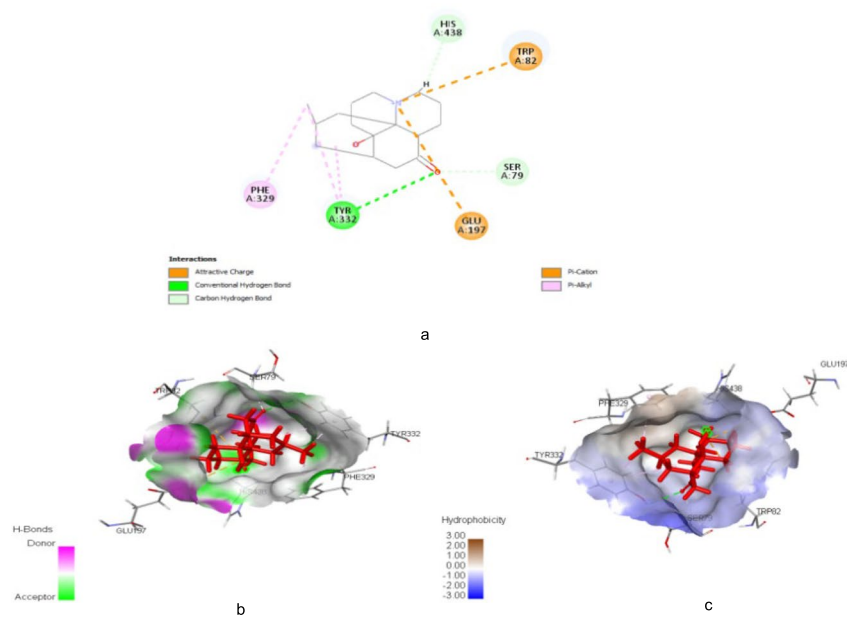
Molecular docking/molecular dynamics simulation

Over a span exceeding three decades, computer-aided methods for drug discovery and design have made substantial contributions to the development of essential bioactive therapeutic molecules, while also anticipating potential derivatives that could enhance their efficacy [53]. Currently, the application of in silico techniques, such as chemoinformatics, molecular modeling, and artificial intelligence (AI), has experienced substantial growth, particularly given the crucial role that understanding the molecular foundations of drug interactions plays in drug discovery [54].

From our findings, in order to screen and find acceptable hits that best fit into the most favorable binding mode having the right geometry and complementarity, four prominent leads from AETt with the lowest SP, XPG and MMGBSA scores (Tables 3 and 4), were docked against human AChE (PDB ID: 4EY7) and BChE (PDB ID: 6QAE) proteins. However, the SP scoring algorithm involves the evaluation of van der Waals, electrostatic, and hydrogen bonding interactions between proteins and the hits [55]. This method is less precise when compared to XPG and the computationally intensive MMGBSA scoring technique [56]. The MMGBSA scoring method combines molecular mechanics and continuum solvation models to calculate energy contributions, resulting in a more accurate determination of binding affinity. More so, research suggests that reduced SP and XPG values are indicative of robust interactions and compatibility between individual ligands and the specific protein target being studied [57]. Remarkably, within this array of compounds, rutin and quercetin exhibited noteworthy binding affinity energies [58]. These computed binding



A: Post-docking analysis of human BChE protein target in complex with quercetin; (a) 2D representation of the human BChE -quercetin complex; (b) Hydrophobic cloud interactions around quercetin; (c) Hydrogen acceptors and donor interactions around quercetin.



B: Post-docking analysis of human BChE protein target in complex with lycodoline; (a) 2D representation of the human BChE -lycodoline complex; (b) hydrophobic cloud interactions around lycodoline; (c) hydrogen acceptors and donor interactions around lycodoline.

Fig. 5 A Post-docking analysis of human BChE protein target in complex with quercetin; **a** 2D representation of the human BChE -quercetin complex; **b** Hydrophobic cloud interactions around quercetin; **c** Hydrogen acceptors and donor interactions around quercetin. **B** Post-docking analysis of human BChE protein target in complex with lycodoline; **a** 2D representation of the human BChE -lycodoline complex; **b** hydrophobic cloud interactions around lycodoline; **c** hydrogen acceptors and donor interactions around lycodoline

energies underscore the potential for enhanced binding capability of these two flavonoids with the respective target proteins, surpassing the effectiveness of the standard drugs lycodoline and scopoletin [59].

Furthermore, the complexes formed by the hits with cholinesterases exhibit notable high binding affinities, including parameters such as VDWAALS, EEL, EGB, ESURF, ΔG_{gas} , ΔG_{solv} , and ΔG_{total} , as revealed by

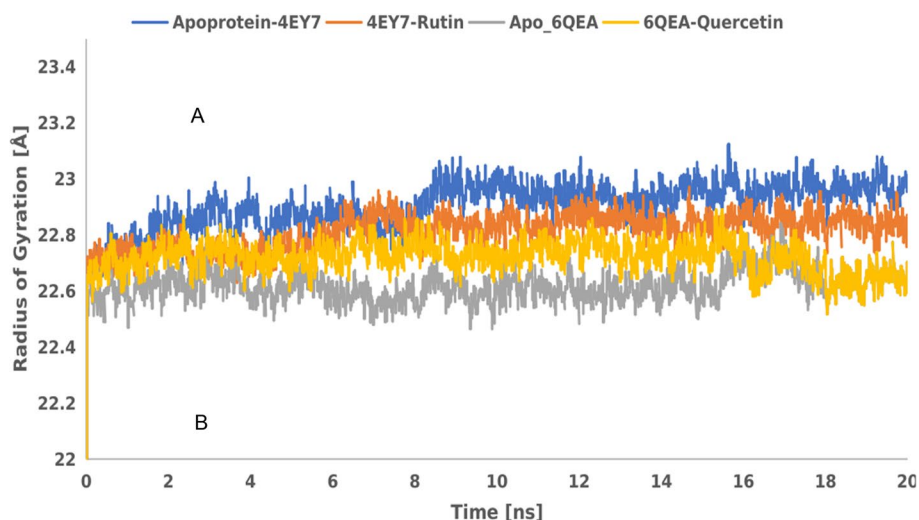
Table 3 Post docking SP, XPG and MMGBSA scores of compounds from the AETt against human butyrylcholinesterase target with Lycodoline as standard

PubMed IUPAC	Docking score	XPG score	MMGBSA dG binding score
Rutin	-12.92	-12.95	-29.28
Quercetin	-10.44	-10.47	-48.36
Luteolin	-9.98	-10.02	-36.77
Kaempferol	-8.84	-8.87	-39.78
Lycodoline	-7.35	-7.53	-50.37

MMGBSA analysis (Fig. 3 a&b). These high binding affinities substantiate the presence of robust and stable interactions between the ligands and respective cholinesterases, which could ultimately translate to the inhibition of their enzymatic activities [60]. This finding supports the viability of these complexes as potential target in drug development [61]. Moreover, these distinct properties can potentially be attributed to the diverse hydrogen and hydrophobic bonding interactions exhibited by the hits with different amino acid residues of the protein targets (illustrated in Figs. 4 (a&b) and 5 (a&b)). This observation is consistent with the findings of Chowdhury et al. [62]. Both the hydrogen bonds and hydrophobic interactions assume pivotal roles in drug discovery and design [63]. Hydrogen bonds are indispensable, not only for facilitating drug-receptor binding but also for influencing a molecule's properties like solubility, distribution, and permeability [64]. Similarly, hydrophobic interactions are vital in determining the binding affinity and selectivity of small molecular drugs for their

target, playing a significant role in biomolecular recognition [65]. Additionally, the hydrogen bond interactions and hydrophobicity of the hits derived from AETt could possibly contribute to the favorable pharmacological ADMET parameters observed for rutin and quercetin, as presented in Table 4 [66]. Research has indicated that compounds possessing acceptable ADMET profiles are more likely to demonstrate effectiveness and safety [67]. Understanding and optimizing these ADMET properties are critical in the drug development process and the kinetics of drug exposure to tissues [68]. The ADMET characteristics of rutin and quercetin demonstrate that these compounds possess drug-like attributes that are safe and non-toxic. This probably suggests their potential usefulness in AD drug development.

Radius of gyration (Rg) is another invaluable parameter used to evaluate the conformational properties of AChE (PDB ID: 4EY7) and BChE (PDB ID: 6QAE) complexation with rutin and quercetin in molecular dynamics simulation. A molecular dynamics simulation provides insights into the conformational dynamics and structural stability of the protein–ligand complex by keeping track of changes in the Rg [69]. The Rg value has been used as a measure of the compactness and stability of protein with ligand [70]. It also quantifies the distribution of the atoms in the complex relative to the centre mass. A more broad or unfolded structure is indicated by an increase in the Rg value than a more compact or folded structure [71]. As seen in our study (Fig. 6), 4EY7-rutin and 6QAE-quercetin indicated moderate Rg value compared to the apo-proteins used. However, 6QAE-quercetin showed a more compacted or folded structures. Similarly,

**Fig. 6** Radius of gyration plot as a function of simulation time-dependent analysis of molecular dynamics trajectory of apo-AChE, AChE-rutin, apo-BChE, and BChE-quercetin complexes

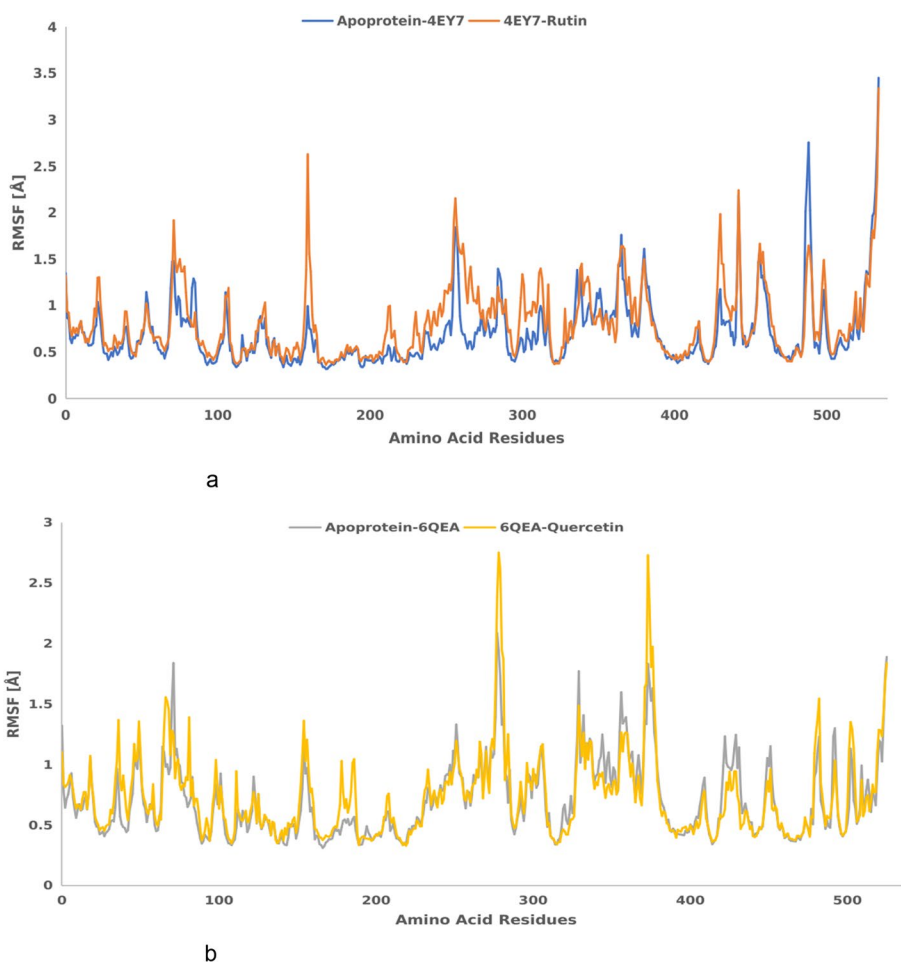


Fig. 7 a&b Root mean square fluctuation of the residues of simulation time dynamics of **a** apo-AChE & AChE-rutin complexes; and **B** apo-BChE & BChE-quercetin complexes

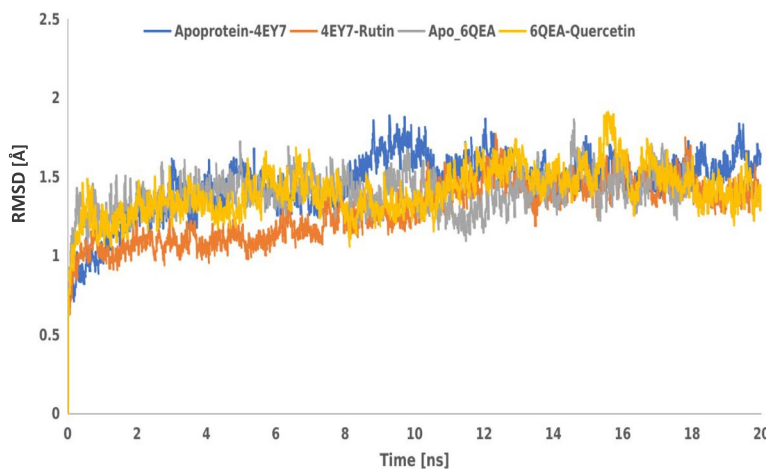


Fig. 8 Root mean square deviation (RMSD) plot as a function of simulation time of rutin and quercetin dynamics binding to acetylcholinesterase (PDB ID: 4EY7) and butyrylcholinesterase (PDB ID: 6QAE)

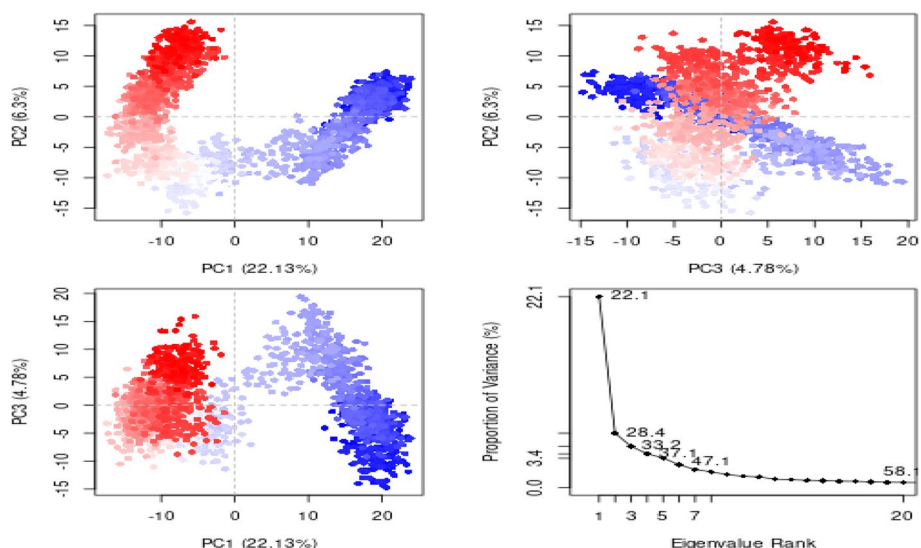


Fig. 9 Interpretation of variance of AChE-rutin complex against eigenvalues calculated by principal component (PC) analysis. PCA trajectory with instantaneous conformations (i.e. trajectory frames) colored from blue to red in order of time. The 3 PCs showed fluctuating regions with 33.78% overall fluctuations. The fluctuations in PC1, PC2 and PC3 were 22.1%, 6.3% and 4.78%, respectively

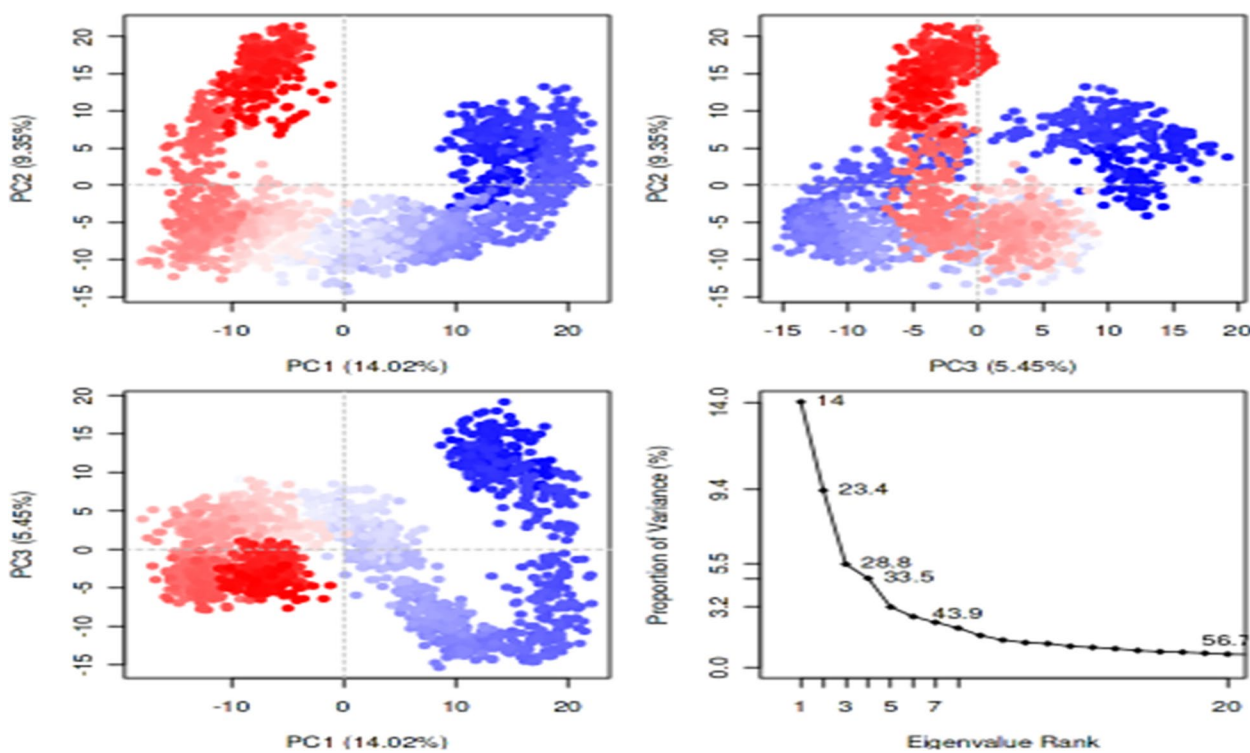


Fig. 10 The interpretation of variance of BChE-quercetin complex against eigenvalues calculated by principal component analysis. PCA trajectory with instantaneous conformations (i.e. trajectory frames) colored from blue to red in order of time. The 3 PCs showed fluctuating regions with 33.78% overall fluctuations. The fluctuations in PC1, PC2 and PC3 were 14.02%, 9.35% and 5.45%, respectively

a more common method for assessing the flexibility and local dynamics of a protein–ligand complex during a molecular dynamics simulation is root mean square

fluctuation (RMSF) analysis [72]. RMSF provides details on the parts of the complex that are more rigid or suffer from large fluctuations [73]. As indicated in Fig. 7 (a&b),

Table 4 ADMET/ADME properties of bioactive lead compounds from the aqueous extract of *Talinum triangulare* leave (AETT)

Compounds	Absorption			Distribution			Metabolism		Excretion		Toxicity		
	Caco-2-Perm	Pgp-inhibitor	Pgp-substrate	HIA	PPB (%)	VD	BBB-Penetration	Inhibitor	Substrate	CL	hERG-Blockers	H-HT	Carcin
Rutin	-6.47	0.005	0.997	0.876	87.1	0.701	0.041	CYP3A4, CYP1A2, CYP2C19, CYP2D6, CYP2C9	CYP2C9, CYP1A2, CYP2C19, CYP3A4, CYP2D6,	1.50	0.227	0.083	0.055
Quercetin	-5.20	< 0.100	< 0.100	< 0.100	95.5	0.580	< 0.100	CYP1A2, CYP2C19, CYP2C9, CYP2D6, CYP3A4	CYP1A2, CYP2C9, CYP2C19, CYP2D6, CYP3A4	8.28	< 0.100	< 0.100	< 0.100

Key: Caco-2 Human colon adenocarcinoma cell lines, Pgp P-glycoprotein, inhibitor or substrate, HIA human intestinal absorption, PPB Plasma protein binding, VD Volume of distribution, BBB-Penetration blood-brain barrier penetration, CYP Cytochrome, CL Clearance, hERG Blockers, H-HT Human hepatotoxicity, Carcin Carcinogenicity

AChE-rutin (4EY7-rutin) complex had the highest RMSF (Å) value compared to other complexes. Lower RMSF values indicate rigid or stable regions, while higher RMSF values suggest regions with greater flexibility or larger structural fluctuations [74]. However, the complexes maintained their stability throughout the simulation, as indicated by the average RMSD values (Fig. 8), which implies profound protein–ligand interactions. The RMSD describes the measure of the changes in the conformation of a given structure over time and offers details on the complexes' long-term stability and convergence.

The protein's structural changes caused by rutin and quercetin dynamics binding were also verified using principal component analysis (PCA) that revealed the overall motion of the molecular dynamics trajectories [75]. As seen in Figs. 9 and 10, the top five eigenvectors in the human AChE and BChE complexes showed dominating movements with eigenvalues between 22.1–47.1% and 14–43.9%, respectively. In general, all clusters showed conformational changes with the blue region presenting the most significant movements, the white region representing intermediate movements, and the red zone showing the least flexible motions, according to the PCA. For the AChE-rutin (Fig. 9), PC1 had the highest variance, followed by PC2 and PC3. This suggests that PC1 captured the most significant structural changes induced by the ligand binding, while PC2 and PC3 captured more subtle changes in the orientation and conformation of

different functional groups [76]. Similarly, for the BChE-quercetin (Fig. 10), PC1 had a lower variance, while PC2 and PC3 had higher variances. This implies that the ligand induced more subtle structural changes in the protein as captured by PC2 and PC3, while PC1 revealed the most significant structural changes according to the report of Laerge and Yonetani [77]. Additionally, investigation of mode similarity analyses between anisotropic network model and C-alpha force fields were revealed using root mean square inner product (RMSIP) in 4EY7-rutin and 6QAE-quercetin. In the plots, the protein residues are displayed as pixels in a heatmap, and the colour of each pixel indicates the RMSIP value for an individual protein residue (Fig. 11 a&b). Darker colour typically corresponds to lower RMSIP values, and this denotes lower similarity between the two force fields' predicted normal modes, whereas lighter colours correspond to higher RMSIP values and similarly denote greater similarity.

Conclusion

Our study investigated the antioxidant (ABTS cation radicals inhibition) and enzyme (cholinesterase and butyrylcholinesterase) inhibitory activities of the aqueous extract of *Talinum triangulare* leaf (AETt). Also, molecular docking and simulation studies were performed to explore the interaction of previously identified bioactive compounds in AETt with human cholinesterase enzymes. The results however, indicated noticeable ABTS radical

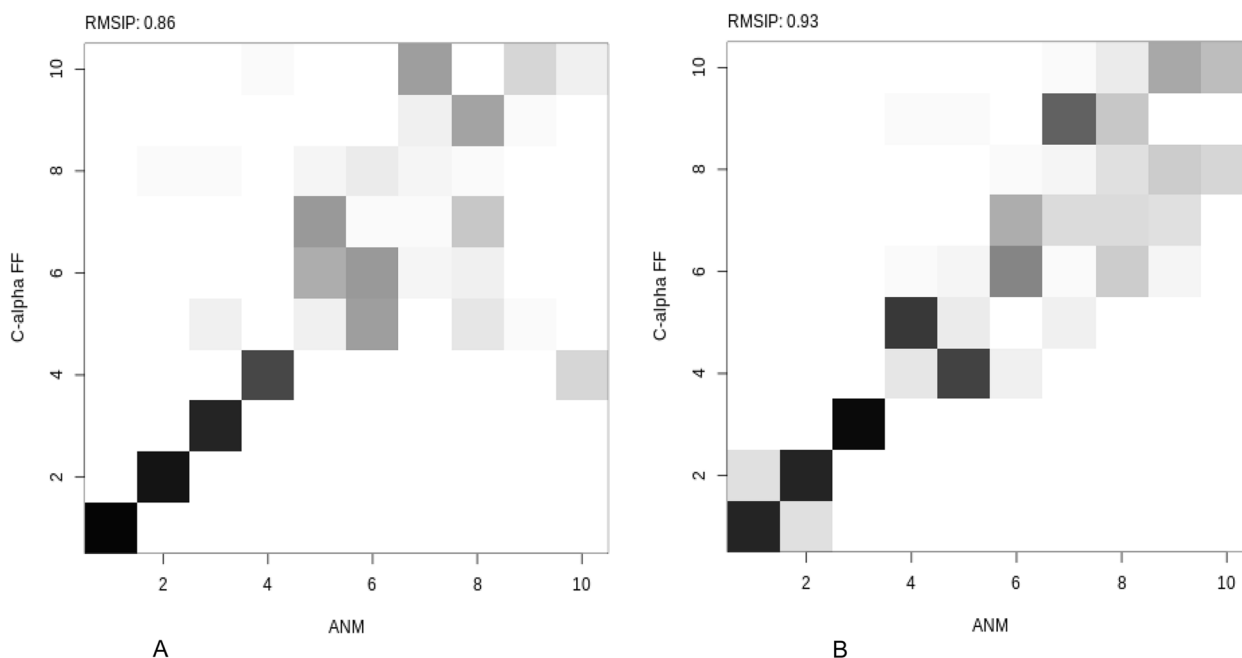


Fig. 11 Mode similarity analyses between anisotropic network model and C-alpha force fields using RMSIP for **A** acetylcholinesterase-rutin complex and **B** butyrylcholinesterase-quercetin complex. ANM, anisotropic network model

and cholinesterase inhibitory activities as exhibited by AETt. More so, molecular docking simulations identified rutin and quercetin from AETt as promising drug candidates, demonstrating strong binding affinities with human cholinesterase enzymes. Also, further computational analyses indicated structural stability, compactness, and stable interactions of the acetylcholinesterase-rutin and butyrylcholinesterase-quercetin complexes. Overall, our study could offer valuable insights into the radical scavenging and cholinesterase inhibitory potential of AETt, thereby providing a premise for drug development useful in the management of Alzheimer's disease.

Abbreviations

µg	Microgramme
Abs	Absorbance
ABTS	2,2'-Azinobis (3-ethyl-benzothiazoline-6-sulfonic acid)
ACh	Acetylcholine
AChE	Acetylcholinesterase
AD	Alzheimer's disease
ADME	Administration, distribution, metabolism and excretion
ADMET	Administration, distribution, metabolism, excretion and toxicity
AETt	Aqueous extract of <i>Talinum triangulare</i> leave
ARG	Arginine
ASP	Aspartic acid
BCh	Butyrylcholine
BChE	Butyrylcholinesterase
BHT	Butylated hydroxytoluene
BHT	Butylated hydroxytoluene
ChE	Cholinesterases
DTNB	5,5'-Dithiobis (2-nitrobenzoic acid)
EC	Enzyme code
EEL	Electrostatic
EGB	Generalized born electrostatic
ESURF	Nonpolar solvation
GB/SA	Generalized-Born/surface area
GLN	Glutamine
GLU	Glutamic acid
GLY	Glycine
HIS	Histidine
HPLC-DAD	High performance liquid chromatography coupled with diode-array detection
IC ₅₀	Concentration that can cause 50% inhibition
LEU	Leucine
m	Molarity
MDS	Molecular dynamics simulation
ml	Milliliter
mM	Millimole
MM-GB/SA	Molecular mechanics/generalized born surface area
PBS	Phosphate buffer Saline
PC	Principal component
PCA	Principal component analysis
PHE	Phenylalanine
Rg	Radius of gyration
RMSF	Root mean square fluctuation
RMSIP	Root mean square inner product
ROS	Reactive oxygen specie
RT	Room temperature
SER	Serine
SP	Standard precision
TRP	Tryptophan
Tt	<i>Talinum triangulare</i>
TYR	Tyrosine
UV	Ultraviolet
VAL	Valine
VDWAALS	Van der Waals

XP	High precision
ΔG	Free energy of binding
ΔG solv	Free energy of solvation
ΔG total	Total free energy of binding

Supplementary Information

The online version contains supplementary material available at <https://doi.org/10.1186/s12906-024-04424-2>.

Supplementary Material 1.

Acknowledgements

The authors hereby appreciate the management of Afe Babalola University for creating an enabling environment for the success of this study and ensuring the public visibility of the publication.

Financial interests

The authors have no relevant financial or non-financial interests to disclose.

Authors' contributions

AOB*, OOR, JFK, OOV, AFD and IOT conceptualized the research; Data curation was carried out by AOB*, OOR & MSO; Formal analysis by AOB*, JFK and OAO; OOR, KFJ, OOV, AFD contributed reagents and analytical tools; AOB* & AOB supervised the study; AOB*, OOR, JFK, OOV, AFD, IOT, AOO, MSO and AOB validated the data; AOB*, OOR, OAO & IOT drafted original manuscript; AOB*, OOR, JFK, OOV, AFD, IOT, OAO, MSO and AOB reviewed, edited and approved final version of the manuscript.

Funding

There was no financial assistance received for the study either from governmental or non-governmental body.

Availability of data and materials

Proteins analyzed such as human acetylcholinesterase (AChE) (PDB ID: 4EY7) and butyrylcholinesterase (BChE) (PDB ID: 6QAE) were obtained from protein data bank (<https://www.rcsb.org/>).

Declarations

Ethics approval and consent to participate

Not applicable.

Consent for publication

Not applicable.

Competing interests

The authors declare no competing interests.

Author details

¹Department of Chemical Sciences, Phytomedicine and Toxicology Unit, College of Sciences, Biochemistry Programme Afe-Babalola University, P.M.B 5454, Ado-Ekiti, Ekiti State, Nigeria. ²Department of Medical Biochemistry, College of Medicine and Health Sciences, Afe Babalola University, P.M.B 5454, Ado-Ekiti, Ekiti State, Nigeria. ³Department of Chemical Sciences, Industrial and Chemical Unit, Industrial Chemistry Programme, College of Sciences, Afe-Babalola University, P.M.B 5454, Ado-Ekiti, Ekiti State, Nigeria. ⁴Department of Biological Sciences, College of Sciences, Afe-Babalola University, P.M.B 5454, Ado-Ekiti, Ekiti State, Nigeria.

Received: 27 September 2023 Accepted: 1 March 2024

Published online: 28 March 2024

References

- Sheladia S, Reddy PH. Age-related chronic diseases and Alzheimer's disease in Texas: a Hispanic focused study. *J Alzheimer Dis Rep.* 2021;5(1):121–33.
- Chen ZR, Huang JB, Yang SL, Hong FF. Role of cholinergic signaling in Alzheimer's disease. *Molecules.* 2022;27(6):1816.

3. Rabbito A, Dulewicz M, Kulczyńska-Przybik A, Mroczko B. Biochemical markers in Alzheimer's disease. *Int J Mol Sci.* 2020;21(6):1989.
4. Association A. 2019 Alzheimer's disease facts and figures. *Alzheimer Dement.* 2019;15(3):321–87.
5. Association A. 2018 Alzheimer's disease facts and figures. *Alzheimer Dement.* 2018;14(3):367–429.
6. Mayeux R, Sano M. Treatment of Alzheimer's disease. *New Eng J Med.* 1999;341(22):1670–9.
7. Winblad B, Amouyel P, Andrieu S, Ballard C, Brayne C, Brodaty H, et al. Defeating Alzheimer's disease and other dementias: a priority for European science and society. *Lancet Neurol.* 2016;15(5):455–532.
8. Association A. 2016 Alzheimer's disease facts and figures. *Alzheimer Dement.* 2016;12(4):459–509.
9. Afolabi OB, Olasehinde OR, Olanipon DG, Mabayoje SO, Familua OM, Jaiyesimi KF, et al. Antioxidant evaluation and computational prediction of prospective drug-like compounds from polyphenolic-rich extract of *Hibiscus cannabinus* L. seed as antidiabetic and neuroprotective targets: assessment through in vitro and in silico studies. *BMC Compl Med Ther.* 2023;23(1):203.
10. Pepeu G, Giovannini MG. The fate of the brain cholinergic neurons in neurodegenerative diseases. *Brain Res.* 2017;1670:173–84.
11. Sultana R, Butterfield DA. Role of oxidative stress in the progression of Alzheimer's disease. *J Alzheimer Dis.* 2010;19(1):341C353.
12. Gülçin İ, Scozzafava A, Supuran CT, Akıncioğlu H, Koksal Z, Turkan F, et al. The effect of caffeic acid phenethyl ester (CAPE) on metabolic enzymes including acetylcholinesterase, butyrylcholinesterase, glutathione S-transferase, lactoperoxidase, and carbonic anhydrase isoenzymes I, II, IX, and XII. *J Enzyme Inhib Med Chem.* 2016;31(6):1095–101.
13. Fahim AM, Farag AM, Mermer A, Bayrak H, Şirin Y. Synthesis of novel β -lactams: antioxidant activity, acetylcholinesterase inhibition and computational studies. *J Mol Struct.* 2021;1233:130092.
14. Abbas S, Latif M, Shafie N, Ghazali M, Abidin N, Mustafa M, et al. A review of antioxidant and anti-acetylcholinesterase activities of *Centella asiatica* (L.) Urb. for the treatment of Alzheimer's disease. *Food Res.* 2021;5(2):1–7.
15. Ali R, Sheikha IA, Jabirb NR, Kamal MA. Comparative review of decade's research on cholinesterase inhibition. *Am J Neuroprot Neuroregen.* 2012;4(2):136–44.
16. Hampel H, Mesulam MM, Cuello AC, Farlow MR, Giacobini E, Grossberg GT, et al. The cholinergic system in the pathophysiology and treatment of Alzheimer's disease. *Brain.* 2018;141(7):1917–33.
17. Poprac P, Jomova K, Simunkova M, Kollar V, Rhodes CJ, Valko M. Targeting free radicals in oxidative stress-related human diseases. *Trend Pharmacol Sci.* 2017;38(7):592–607.
18. Marucci G, Buccioni M, Dal Ben D, Lambertucci C, Volpini R, Amenta F. Efficacy of acetylcholinesterase inhibitors in Alzheimer's disease. *Neuropharmacol.* 2021;190: 108352.
19. Tayeb HO, Yang HD, Price BH, Tarazi FI. Pharmacotherapies for Alzheimer's disease: beyond cholinesterase inhibitors. *Pharmacol Ther.* 2012;134(1):8–25.
20. Haruna A, Yahaya SM. Recent advances in the chemistry of bioactive compounds from plants and soil microbes: A review. *Chem Afr.* 2021;4(2):231–48.
21. Subramanian MS, Nandagopal MSG, Amin Nordin S, Thilakavathy K, Joseph N. Prevailing knowledge on the bioavailability and biological activities of sulphur compounds from Alliums: A potential drug candidate. *Molecules.* 2020;25(18):4111.
22. Pisoschi AM, Pop A, Iordache F, Stanca L, Predoi G, Serban AI. Oxidative stress mitigation by antioxidants-an overview on their chemistry and influences on health status. *Eur J Med Chem.* 2021;209: 112891.
23. Oluwole SO, Ogun ML, Durowoju SY. Effects of Different Organic Manures on the Growth of Water Leaf (*Talinum triangulare* Jacq). *Int J Inn Sci Res Tech.* 2019;4(5):1123–9.
24. Dinesh A, Kumar A. A review on bioactive compounds, ethnomedicinal importance and pharmacological activities of *Talinum triangulare* (Jacq.) Willd. *Chem Biodivers.* 2023;20(12):e202301079.
25. Afolabi OB, Oloyede OI, Agunbiade OS, Obafemi TO, Aline B, Obajuluwa A, et al. HPLC-DAD profiling and inhibitory potentials of ethylacetate and aqueous extracts of *Talinum triangulare* on key enzymes linked to type-2 diabetes (α -amylase and α -glucosidase) and oxidative stress (monoamine oxidase). *Egypt J Basic Appl Sci.* 2019;6(1):99–110.
26. Afolabi OB, Oloyede OI, Olayide II, Obafemi TO, Awe OJ, Afolabi BA, et al. Antioxidant enhancing ability of different solvents extractable components of *Talinum triangulare* in some selected Tissue homogenates of Albino Rats-In vitro. *J Appl Pharm Sci.* 2015;5(9):56–61.
27. Enogieru AB, Momodu OI. African medicinal plants useful for cognition and memory: Therapeutic implications for Alzheimer's disease. *Bot Rev.* 2021;87:107–34.
28. Igbayilola YD, Morakinyo AO, Ewetayo AW, Oyabambi AO, Saka WA. Biochemical and antioxidant effects of *Talinum triangulare* (Water Leaf) in female Sprague-Dawley rats. *Int J Basic Appl Physiol.* 2017;6(1):22–8.
29. Morrison JF, Twumasi SK. Comparative studies on the in vitro antioxidant properties of methanolic and hydro-ethanolic leafy extracts from eight edible leafy vegetables of Ghana. *Afr J Biotechnol.* 2010;9(32):5177–84.
30. Afolabi OB, Oloyede OI. Antioxidant properties of the extracts of *Talinum triangulare* and its effect on antioxidant enzymes in tissue homogenate of Swiss albino rat. *Toxicol Int.* 2014;21(3):307.
31. Miller NJ, Rice-Evans C, Davies MJ, Gopinathan V, Milner A. A novel method for measuring antioxidant capacity and its application to monitoring the antioxidant status in premature neonates. *Clin Sci.* 1993;84(4):407–12.
32. Ellman GL, Courtney KD, Andres V, Featherstone RM. A new and rapid colorimetric determination of acetylcholinesterase activity. *Biochem Pharmacol.* 1961;7:88–95.
33. Mahmoud DE, Faraag AH, Abu El-Wafa WM. *In vitro* study on the potential fungicidal effects of atorvastatin in combination with some azole drugs against multidrug resistant *Candida albicans*. *World J Microbiol Biotechnol.* 2021;37(11):1–3.
34. Tripathi SK, Muttineni R, Singh SK. Extra precision docking, free energy calculation and molecular dynamics simulation studies of CDK2 inhibitors. *J Theor Biol.* 2013;334:87–100.
35. Halgren TA, Murphy RB, Friesner RA, Beard HS, Frye LL, Pollard WT, et al. Glide: a new approach for rapid, accurate docking and scoring. 2. Enrichment factors in database screening. *J Med Chem.* 2004;47(7):1750–9.
36. Friesner RA, Banks JL, Murphy RB, Halgren TA, Klicic JJ, Mainz DT, et al. Glide: a new approach for rapid, accurate docking and scoring. 1. Method and assessment of docking accuracy. *J Med Chem.* 2004;47(7):1739–49.
37. Lyne PD, Lamb ML, Saeh JC. Accurate prediction of the relative potencies of members of a series of kinase inhibitors using molecular docking and MM-GBSA scoring. *J Med Chem.* 2006;49(16):4805–8.
38. Daina A, Michielin O, Zoete V. SwissADME: a free web tool to evaluate pharmacokinetics, drug-likeness and medicinal chemistry friendliness of small molecules. *Sci Rep.* 2017;7(1):42717.
39. Lemkul J. From proteins to perturbed Hamiltonians: A suite of tutorials for the GROMACS-2018 molecular simulation package. *Living J Comp Mol Sci.* 2019;1(1):5068.
40. Süntar I. Importance of ethnopharmacological studies in drug discovery: role of medicinal plants. *Phytochem Rev.* 2020;19(5):199–209.
41. Balsano C, Alisi A. Antioxidant effects of natural bioactive compounds. *Curr Pharm Des.* 2009;15(26):3063–73.
42. Giasson BI, Ischiropoulos H, Lee VM, Trojanowski JQ. The relationship between oxidative/nitrative stress and pathological inclusions in Alzheimer's and Parkinson's diseases. *Free Radic Biol Med.* 2002;32(12):1264–75.
43. Simunkova M, Alwasel SH, Alhazza IM, Jomova K, Kollar V, Rusko M, et al. Management of oxidative stress and other pathologies in Alzheimer's disease. *Arch Toxicol.* 2019;93:2491–513.
44. Yu M, Gouvinhas I, Rocha J, Barros AI. Phytochemical and antioxidant analysis of medicinal and food plants towards bioactive food and pharmaceutical resources. *Sci Rep.* 2021;11(1):10041.
45. Ismail HF, Hashim Z, Soon WT, Ab Rahman NS, Zainudin AN, Majid FA. Comparative study of herbal plants on the phenolic and flavonoid content, antioxidant activities and toxicity on cells and zebrafish embryo. *J Trad Compl Med.* 2017;7(4):452–65.
46. Sánchez-Moreno C. Methods used to evaluate the free radical scavenging activity in foods and biological systems. *Food Sci Tech Int.* 2002;8(3):121–37.
47. Müller L, Fröhlich K, Böhm V. Comparative antioxidant activities of carotenoids measured by ferric reducing antioxidant power (FRAP), ABTS bleaching assay (ATEAC), DPPH assay and peroxy radical scavenging assay. *Food Chem.* 2011;129(1):139–48.
48. Dastmalchi K, Dorman HD, Koşar M, Hiltunen R. Chemical composition and in vitro antioxidant evaluation of a water-soluble Moldavian balm (*Dracocephalum moldavica* L.) extract. *LWT-Food Sci Tech.* 2007;40(2):239–48.

49. Kumar A, Pintus F, Di Petrillo A, Medda R, Caria P, Matos MJ, et al. Novel 2-phenylbenzofuran derivatives as selective butyrylcholinesterase inhibitors for Alzheimer's disease. *Sci Rep*. 2018;8(1):4424.
50. Tripathi A, Srivastava UC. Acetylcholinesterase: a versatile enzyme of nervous system. *Ann Neurosci*. 2010;15(4):106–11.
51. Haake A, Nguyen K, Friedman L, Chakkampambal B, Grossberg GT. An update on the utility and safety of cholinesterase inhibitors for the treatment of Alzheimer's disease. *Exp Opin Drug Saf*. 2020;19(2):147–57.
52. Bari WU, Zahoor M, Zeb A, Khan I, Nazir Y, Khan A, et al. Anticholinesterase, antioxidant potentials, and molecular docking studies of isolated bioactive compounds from *Grewia optiva*. *Int J Food Prop*. 2019;22(1):1386–96.
53. Lešnik S, Štular T, Brus B, Knez D, Gobec S, Janežic D, et al. LiSiCA: a software for ligand-based virtual screening and its application for the discovery of butyrylcholinesterase inhibitors. *J Chem Inf Model*. 2015;55(8):1521–8.
54. Sliwowski G, Kothiwale S, Meiler J, Lowe EW. Computational methods in drug discovery. *Pharmacol Rev*. 2014;66(1):334–95.
55. Meng XY, Zhang HX, Mezei M, Cui M. Molecular docking: a powerful approach for structure-based drug discovery. *Curr Comput Aided Drug Des*. 2011;7(2):146–57.
56. Aamir M, Singh VK, Dubey MK, Meena M, Kashyap SP, Katari SK, et al. In silico prediction, characterization, molecular docking, and dynamic studies on fungal SDRs as novel targets for searching potential fungicides against *Fusarium* wilt in tomato. *Front Pharmacol*. 2018;9:1038.
57. Repasky MP, Shelley M, Friesner RA. Flexible ligand docking with Glide. *Curr Protoc Bioinform*. 2007;18(1):8–12.
58. Taylor DE, Strawhecker KE, Shanholtz ER, Sorescu DC, Sausa RC. Investigations of the intermolecular forces between RDX and polyethylene by force–distance spectroscopy and molecular dynamics simulations. *J Phys Chem A*. 2014;118(27):5083–97.
59. Haldane A, Manhart M, Morozov AV. Biophysical fitness landscapes for transcription factor binding sites. *PLoS Comput Biol*. 2014;10(7):e1003683.
60. Leon R, Garcia AG, Marco-Contelles J. Recent advances in the multitarget-directed ligands approach for the treatment of Alzheimer's disease. *Med Res Rev*. 2013;33(1):139–89.
61. Mirza MU, Froeyen M. Structural elucidation of SARS-CoV-2 vital proteins: Computational methods reveal potential drug candidates against main protease, Nsp12 polymerase and Nsp13 helicase. *J Pharm Anal*. 2020;10(4):320–8.
62. Chowdhury KH, Chowdhury MR, Mahmud S, Tareq AM, Hanif NB, Banu N, et al. Drug repurposing approach against novel coronavirus disease (COVID-19) through virtual screening targeting SARS-CoV-2 main protease. *Biology*. 2020;10(1):2.
63. Brunetti L, Leuci R, Carrieri A, Catto M, Occhineri S, Vinci G, et al. Structure-based design of novel donepezil-like hybrids for a multi-target approach to the therapy of Alzheimer's disease. *Eur J Med Chem*. 2022;237: 114358.
64. Wang Y, Peng C, Wang G, Xu Z, Luo Y, Wang J, et al. Exploring binding mechanisms of VEGFR2 with three drugs lenvatinib, sorafenib, and sunitinib by molecular dynamics simulation and free energy calculation. *Chem Biol Drug Des*. 2019;93(5):934–48.
65. Feixas F, Lindert S, Sinko W, McCammon JA. Exploring the role of receptor flexibility in structure-based drug discovery. *Biophys Chem*. 2014;186:31–45.
66. Razzaghi-Asl N, Mirzayi S, Mahnam K, Sepehri S. Identification of COX-2 inhibitors via structure-based virtual screening and molecular dynamics simulation. *J Mol Graph Model*. 2018;83:138–52.
67. Singh S, Sk MF, Sonawane A, Kar P, Sadhukhan S. Plant-derived natural polyphenols as potential antiviral drugs against SARS-CoV-2 via RNA-dependent RNA polymerase (RdRp) inhibition: an in-silico analysis. *J Biomol Struct Dyn*. 2021;39(16):6249–64.
68. Gleeson MP, Hersey A, Montanari D, Overington J. Probing the links between in vitro potency, ADMET and physicochemical parameters. *Nat Rev Drug Discov*. 2011;10(3):197–208.
69. Boonma T, Soikudrua N, Nutho B, Rungrotmongkol T, Nunthaboot N. Insights into binding molecular mechanism of hemagglutinin H₃N₂ of influenza virus complexed with arbidol and its derivative: A molecular dynamics simulation perspective. *Comput Biol Chem*. 2022;101:107764.
70. Baammi S, Daoud R, El Allali A. In silico protein engineering shows that novel mutations affecting NAD⁺ binding sites may improve phosphite dehydrogenase stability and activity. *Sci Rep*. 2023;13(1):1878.
71. Best RB, Mittal J. Protein simulations with an optimized water model: cooperative helix formation and temperature-induced unfolded state collapse. *The J Phys Chem B*. 2010;114(46):14916–23.
72. Ahamad S, Gupta D, Kumar V. Targeting SARS-CoV-2 nucleocapsid oligomerization: insights from molecular docking and molecular dynamics simulations. *J Biomol Struct Dyn*. 2022;40(6):2430–43.
73. Berhanu WM, Masunov AE. Molecular dynamic simulation of wild type and mutants of the polymorphic amyloid NNQNTF segments of elk prion: structural stability and thermodynamic of association. *Biopolymers*. 2011;95(9):573–90.
74. Butterfield DA, Boyd-Kimball D. Oxidative stress, amyloid-β peptide, and altered key molecular pathways in the pathogenesis and progression of Alzheimer's disease. *J Alzheimer Dis*. 2018;62(3):1345–67.
75. Lolok N, Sumiwi SA, Muhtadi A, Susilawati Y, Hendriani R, Ramadhan DS, et al. Molecular docking and molecular dynamics studies of bioactive compounds contained in noni fruit (*Morinda citrifolia* L.) against human pancreatic α-amylase. *J Biomol Struct Dyn*. 2022;40(15):7091–8.
76. Quaray Z, ElSawy KM, Lane DP, Essex JW, Verma C. Reactivation of mutant p53: Constraints on mechanism highlighted by principal component analysis of the DNA binding domain. *Proteins*. 2016;84(10):1443–61.
77. Laberge M, Yonetani T. Molecular dynamics simulations of hemoglobin A in different states and bound to DPG: effector-linked perturbation of tertiary conformations and HbA concerted dynamics. *Biophys J*. 2008;94(7):2737–51.

Publisher's Note

Springer Nature remains neutral with regard to jurisdictional claims in published maps and institutional affiliations.